Variational Myocardial Tracking from Cine-MRI with Non-linear Regularization: Validation of Radial Displacements vs. Tagged-MRI

Viateur Tuyisenge, Adélaïde Albouy-Kissi, and Laurent Sarry

Clermont Université, Université d' Auvergne, ISIT UMR 6284 UdA-CNRS
Clermont-Ferrand, France
{viateur.tuyisenge,adelaide.kissi,laurent.sarry}@udamail.fr

Abstract. We present a new motion estimation approach for cardiac Magnetic Resonance Imaging (Cine-MRI) data from variational framework. The improved performance of this variational approach has been achieved by designing a new regularization term that properly handles motion discontinuities. This approach was applied to both synthetic and real data. The quantitative evaluation revealed that the results of proposed method on cine-MRI correlates with the results given by inTag[1], reference approach on tagged-MRI.

1 Introduction

Non-invasive image-based analysis and quantification of cardiac motion provide important information of how a pathology affects local and global deformation of the myocardium and its responses to a given therapy. The estimation of myocardium deformations helps to detect its regions with abnormal contraction in order to provide curative measures for recovery.

The accurate evaluation of the myocardium displacement plays an important role to assess the regional function of myocardium in measuring the regional strain. Several approaches have been proposed [2, 5, 10, 13] and references therein, to address the problem of velocity measurement of myocardium from the available imaging modalities. However, there is still lack of methods that determine reliably the variations of transmural movement of the heart.

We propose a dense velocity field estimation in a variational framework which consists of data term and regularization term to address this problem. In this regard, we adopted a data term that resides on standard principle of pixel intensity conservation of a moving point and regularization term has been designed to account for the motion discontinuities accurately.

2 Method

The problem of motion estimation dates for more than two decades. Since the time, Horn and Schunck [8], Lukas Kanade (1981) up to now, many researchers

[1] *inTag* is an open-source OsiriX plugin developed by the CREATIS laboratory (http://www.creatis.insa-lyon.fr/inTag/).

S. Ourselin, D. Rueckert, and N. Smith (Eds.): FIMH 2013, LNCS 7945, pp. 334–341, 2013.

continued to address this problem in different ways as surveyed by Mitiche and Bouthemy [11], Stiller and Kornad [14], Weickert et al. [18] among others. Many experiments proved superior performance of the variational motion estimation approaches [1, 3]. These approaches rely on standard principle of intensity conservation between consecutive frames separated by a short time intervals.

Let $I(x(t), y(t), t)$ be the intensity of pixel $(x(t), y(t))$ at time t, the intensity conservation principle can be formulated as follows: $\frac{dI(x(t),y(t),t)}{dt} = 0$. Applying chain differentiation rule leads to the following common optical flow constrain equation (OFCE): $I_x u + I_y v + I_t = 0$, where I_x and I_y denote spatial derivatives in x and y directions, I_t temporal derivatives and $(u = \frac{\partial x}{\partial t}, v = \frac{\partial y}{\partial t})$ velocity field to compute.

However such a single equation is not sufficient to determine two unknowns u and v uniquely for each pixel. If used alone, it only allows to compute the flow component parallel to ∇I, known as normal flow. For this, an arbitrary tangential components might be added to satisfy the optical flow constraint. This ambiguity illustrates the ill-posedness of optical flow computation formulated in terms of the OFCE commonly known as aperture problem. Thus, additional regularization assumption is needed to recover a unique flow field.

Horn and Schunck [8] proposed the regularization that consists in assuming that the flow field varies smoothly in space. They introduced quadratic smoothing of flow field requiring the following integral $\int_\Omega \left(\|\nabla u\|^2 + \|\nabla v\|^2\right) d\Omega$ to be close to 0, Ω stands for image domain. Considering $\mathbf{w} \equiv (u, v)^T$, the flow field is computed as follows:

$$(u, v) = \text{argmin}_{(u,v)} \int_\Omega \left((\nabla I.\mathbf{w} + I_t)^2 + \alpha \|\nabla \mathbf{w}\|^2 \right) d\Omega, \tag{1}$$

where α is a weighting parameter between data term and smoothing term. Unfortunately, the introduction of a quadratic smoothing leads to a continuous and a smoothed solution for the flow field i.e, a solution where discontinuities are destroyed. This is not an accurate solution in case one wants to preserve the flow discontinuities and recover the flow field as accurately as possible. Such discontinuities are present in cardiac imaging and it is much important to find the reliable variations of transmural movement of heart.

Several researchers addressed the flow discontinuity problem using non-quadric smoothing terms, like Nagel [12], Cohen [6], Deriche et al. [7], Weickert [17]. We have investigated the significance of these non-quadratic smoothing terms mathematically, releasing their pros and cons and came up with a new smoothing term that solves encountered problems.

The method proposed by Nagel is related to an image driven smoothness, whereby diffusion across image boundaries with large gradient is reduced. Nagel's approach may misestimate flow discontinuities since they do not always coincide with image ones. Cohen's approach uses L^1 norm minimization related to total variation as image restoration. This approach has been widely used in different applications [4]. Although the approach preserves flow discontinuities, the mathematical analysis revealed that it performs flow field smoothing only in direction parallel to isophotes, which is unsuitable in homogeneous regions.

The non-quadratic smoothing approaches of Deriche and Weickert are related to non-linear diffusion filtering and handle flow discontinuities. However, the user has to ensure that the diffusion effects along the flow gradient are much smaller than those associated with the diffusion along the isophotes for an inhomogeneous regions. This seems difficult to manage during numerical implementation.

2.1 Proposed Approach

We propose a new approach that provides the flow field smoothing accurately. This is achieved by designing a regularization term that will simultaneously act as both quadratic and total variation smoothing; i.e, the area with homogeneous fields will be smoothed isotropically, while the area with high flow gradient, smoothing across boundary will be stopped, keeping the one along the isophote. We derive our approach starting from the following general equation:

$$(u, v) = \operatorname{argmin} \int_{\Omega} \left((\nabla I.\mathbf{w} + I_t)^2 + \alpha\, \Phi(\| \nabla \mathbf{w} \|) \right) d\Omega, \tag{2}$$

where Φ is a robust function that helps to preserve the flow discontinuities. This minimization is performed by Euler-Lagrange formulation, leading to the following equation:

$$\begin{cases} div\left(\frac{\Phi'(\|\nabla u\|)}{\|\nabla u\|}\nabla u\right) = 2\alpha(I_x u + I_y v + I_t)I_x, \\ div\left(\frac{\Phi'(\|\nabla v\|)}{\|\nabla v\|}\nabla v\right) = 2\alpha(I_x u + I_y v + I_t)I_y. \end{cases} \tag{3}$$

Let $\frac{\Phi'(\|\nabla u\|)}{\|\nabla u\|} = g(\|\nabla u\|)$, the divergence term can be expanded as follows:

$$\begin{aligned} div\left(\frac{\Phi'(\|\nabla u\|)}{\|\nabla u\|}\nabla u\right) &= \frac{\partial}{\partial x}\left(g(\|\nabla u\|)u_x\right) + \frac{\partial}{\partial y}\left(g(\|\nabla u\|)u_y\right) \\ &= \frac{g'(\|\nabla u\|)}{\|\nabla u\|}\left(u_x^2 u_{xx} + u_x u_y u_{xy}\right) + u_{xx}\, g(\|\nabla u\|) \\ &\quad + \frac{g'(\|\nabla u\|)}{\|\nabla u\|}\left(u_y^2 u_{yy} + u_x u_y u_{xy}\right) + u_{yy}\, g(\|\nabla u\|) \\ = g'(\|\nabla u\|)\frac{u_x^2 u_{xx} + 2u_x u_y u_{xy} + u_y^2 u_{yy}}{\|\nabla u\|} &+ g(\|\nabla u\|)\left(u_{xx} + u_{yy}\right). \end{aligned} \tag{4}$$

In Gauge coordinate system $\boldsymbol{\eta}$ and $\boldsymbol{\xi}$, with $\boldsymbol{\eta} = \frac{\nabla u}{\|\nabla u\|}$, a unit vector normal to the flow gradient and $\boldsymbol{\xi}^T$. $\boldsymbol{\eta} = 0$, we can compute $u_{\eta\eta} = \frac{\partial^2 u}{\partial \eta^2} = \nabla\left(\nabla u.\boldsymbol{\eta}\right).\boldsymbol{\eta} = \frac{u_x^2 u_{xx} + 2u_x u_y u_{xy} + u_y^2 u_{yy}}{u_x^2 + u_y^2}$ and $u_{\xi\xi} = \frac{\partial^2 u}{\partial \xi^2} = \nabla\left(\nabla u.\boldsymbol{\xi}\right).\boldsymbol{\xi} = \frac{u_y^2 u_{xx} - 2u_x u_y u_{xy} + u_x^2 u_{yy}}{u_x^2 + u_y^2}$. Equation (4) can be written as follows:

$$\begin{aligned} div\left(\frac{\Phi'(\|\nabla u\|)}{\|\nabla u\|}\nabla u\right) &= g'(\|\nabla u\|)\left(\|\nabla u\|\right) u_{\eta\eta} + g(\|\nabla u\|)\left(u_{\eta\eta} + u_{\xi\xi}\right) \\ &= \left[\|\nabla u\|\, g'(\|\nabla u\|) + g(\|\nabla u\|)\right] u_{\eta\eta} + g(\|\nabla u\|)\, u_{\xi\xi}. \end{aligned} \tag{5}$$

Since $g(\|\nabla u\|) = \frac{\Phi'(\|\nabla u\|)}{\|\nabla u\|}$, $g'(\|\nabla u\|) = \frac{\Phi''(\|\nabla u\|)}{\|\nabla u\|} - \frac{\Phi'(\|\nabla u\|)}{\|\nabla u\|^2}$. Replacing g and g' with their proper values in (5), we have the following equation:

$$div\left(\frac{\Phi'(\|\nabla u\|)}{\|\nabla u\|}\nabla u\right) = \left[\frac{\Phi'(\|\nabla u\|)}{\|\nabla u\|} + \|\nabla u\|\left(\frac{\Phi''(\|\nabla u\|)}{\|\nabla u\|} - \frac{\Phi'(\|\nabla u\|)}{\|\nabla u\|^2}\right)\right]u_{\eta\eta} + \frac{\Phi'(\|\nabla u\|)}{\|\nabla u\|}u_{\xi\xi}$$

$$div\left(\frac{\Phi'(\|\nabla u\|)}{\|\nabla u\|}\nabla u\right) = \Phi''(\|\nabla u\|)u_{\eta\eta} + \frac{\Phi'(\|\nabla u\|)}{\|\nabla u\|}u_{\xi\xi}. \quad (6)$$

Equation (6) states that flow field smoothing is done simultaneously in two directions, one in direction $\boldsymbol{\eta}$ with weight $\Phi''(\|\nabla u\|)$, and the other in direction $\boldsymbol{\xi}$ with weight $\frac{\Phi'(\|\nabla u\|)}{\|\nabla u\|}$.

The key idea here is to fix the smoothing weight in direction $\boldsymbol{\eta}$ and $\boldsymbol{\xi}$ in such way that flow fields are smoothed properly without destroying the discontinuities. This can be solved iteratively using non-linear diffusion equation:

$$\frac{\partial u}{\partial t} = h(\|\nabla u\|)u_{\eta\eta} + u_{\xi\xi}, \quad (7)$$

where $h(s)$ is a decreasing function, for instance $h(s) = \exp^{-(\frac{s^2}{2k^2})}$. The parameter k is the contrast factor that controls the level of smoothing and it can be either fixed by hand or automatically by parameter optimization techniques; s denotes the norm of gradient flow [15]. Due to the limited space, the interested reader may refer to [7] and references therein, for more details about the diffusion functions. The weighting function $h(s)$ controls the smoothness of the flow field as follows:

- In region where flow gradient is high, the smoothing effect along its normal direction will be stopped, i.e. $h(s) \to 0$ as $s \to \infty$. This leads to the flow discontinuity preservation: $u_t = \mathbf{w}_{\xi\xi}$.
- In homogeneous region, i.e. areas with small flow gradients, the smoothing is done isotropically because $h(s) \to 1$ as $s \to 0$: $u_t = u_{\eta\eta} + u_{\xi\xi} = \triangle u$, where $\triangle = \frac{\partial^2}{\partial\eta^2} + \frac{\partial^2}{\partial\xi^2}$ is the Laplacian operator.

Finally, combining the optical flow constraint equation and the above smoothing term, after Euler-Lagrange equation, the proposed approach leads to the following equations:

$$\begin{cases} h(\|\nabla u\|)u_{\eta\eta} + u_{\xi\xi} = 2\alpha(I_x u + I_y v + I_t)I_x, \\ h(\|\nabla v\|)v_{\eta\eta} + v_{\xi\xi} = 2\alpha(I_x u + I_y v + I_t)I_y. \end{cases} \quad (8)$$

This large system of equations has been implemented numerically by Gauss-Seidel relaxation method to move iteratively towards the solution of this problem.

2.2 Parameters Optimization

The proposed approach shows also how to tune parameters α and k to get accurate results. Those parameters have been optimized by minimizing the error

Algorithm 1. Gradient descent algorithm to find optimum values for α and k

1. initialization:
$\alpha \leftarrow \alpha_0$;
$k \leftarrow k_0$;
2. Compute: (u, v) with equation (8);
3. Evaluate: $\varepsilon_m(\alpha, k) = \|\Xi(u, v) - \Xi_{Gtr}(u, v)\|^2$;
while $\varepsilon_m >$ Error Tolerance **do**
4. Compute: $\left(\frac{\partial \varepsilon_m}{\partial \alpha}, \frac{\partial \varepsilon_m}{\partial k}\right)$;
5. Update $\alpha \leftarrow \alpha - \Delta t \times \frac{\partial \varepsilon_m}{\partial \alpha}$; ($\Delta t$ is the step size of gradient descent)
6. Update $k \leftarrow k - \Delta t \times \frac{\partial \varepsilon_m}{\partial k}$;
7. Repeat number 2;
8. Repeat number 3;
end while

cost function between the estimated flow field $\Xi(u, v)$ and the ground-truth $\Xi_{Gtr}(u, v)$ as explained in algorithm (1).

The implementation was performed by writing a function to estimate flow field from equations (8) and the Matlab ® (MathWorks, Natick, Massachussets, US) function *fminunc*, was used to compute the global minimum of the error with respect to ground truth.

2.3 Validation Protocol of the Estimated Field

In our previous initial work [16], a comparative study against optical flow methods in literature proved the superior performance of our method. This time, the proposed approach on cine-MRI is evaluated against the flow field computed with inTag on tagged-MRI, considered as gold standard. Since acquisition systems of cine-MRI and tagged-MRI on a subject are not properly synchronised, we opted to use the slices acquired at the same position, with trigger times as close as possible. The evaluation was only performed for radial displacements as our approach is for now not designed to recover properly circumferential field component (no spatial gradients exist in that direction).

2.4 Experiments

The experimental evaluations were performed on synthetic and real datasets. The proposed method in previous section has been compared with results given by inTag.

Experiments with Synthetic Data: the first experimental evaluations were performed on synthetic data. The simulated data were generated using the following transport equation: $\frac{\partial \varphi}{\partial t} + \mathbf{w}\nabla\varphi = 0$. Using this equation, in which a reference image and a known radial displacement field were given as inputs, we have got a deformed image as output. Afterwards, the flow field was computed between the reference image and the deformed image using the proposed method. Note that

the transport equation was implemented numerically using a third order upwind scheme for its stable and non-diffusing solution among others.

Experiments with Real Dataset: the proposed method has been also applied to real cardiac MRI images from 5 subjects and the comparison has been made with results of inTag on tagged-MRI from the same subjects. Figure (1 : b) shows that results are visually satisfying since displacement fields are mainly significant over myocardium and globally divergent.

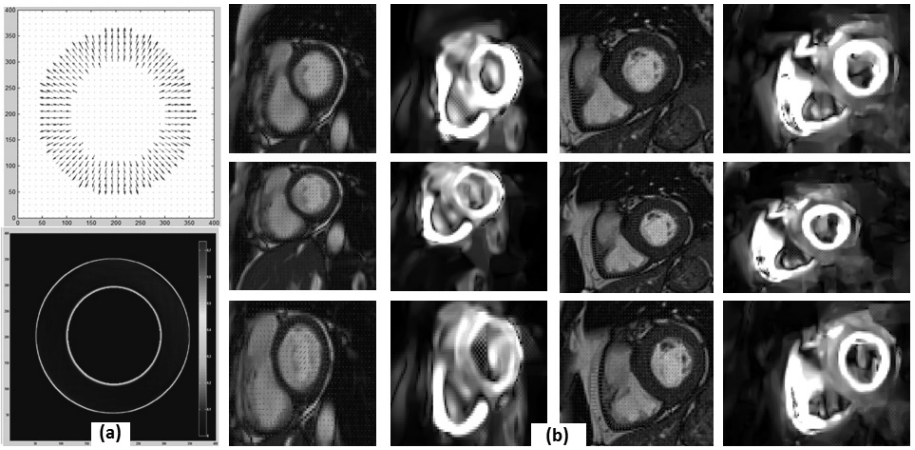

Fig. 1. Experimental results on simulated data and real cardiac MRI images: (a) superposition of the simulated flow field in blue with the estimated one in red (top left) and the corresponding error in magnitude (bottom left) (optimum values $\alpha = 0.0021$ and $k = 0.20$); (b) flow field in red and amplitude estimated from two cine-MRI datasets (middle and right) (optimal values $\alpha = 0.008$ and $k = 0.02$).

2.5 Performance Evaluation

The performance of methods for flow field estimation is quantitatively evaluated by a so-called angular error as proposed by Barron et al. [3]. This is the angle between the true flow and flow estimated by method to quantify. The angular error is computed as follows:

$$\mathbf{Err_{ang}} = \frac{1}{n}\sum_{i=1}^{n} \arccos\left(\frac{\mathbf{w}_e.\mathbf{w}_c}{\|\mathbf{w}_e\|\|\mathbf{w}_c\|}\right), \tag{9}$$

where $\mathbf{w}_e$ is the estimated flow field, $\mathbf{w}_c$ the ground-truth and n represents the total number of pixels. The calculation of the relative magnitude error associated with flow field estimation is an additional measure proposed by Yeon et al. in [9]. Its calculation is done by the following equation:

$$\mathbf{Err_{vel}} = \frac{1}{n} \frac{\sum_{i=1}^{n} |\|\mathbf{w}_e\| - \|\mathbf{w}_c\||}{\|\mathbf{w}_c\|}. \tag{10}$$

In table (1), $\mathrm{Err_{vel}}$ stands for the relative magnitude error computed on real estimated fields and $\mathrm{Err_{vel-rad}}$, the relative magnitude error computed on projected fields in radial reference frame.

Table 1. Quantitative evaluation of the proposed method vs. simulated flow and the ground truth provided by the inTag software for tagged-MRI. Angular error $\mathrm{Err_{ang}}$ is expressed in degrees.

Dataset	$\mathrm{Err_{ang}}$ (°)	$\mathrm{std_{ang}}$	$\mathrm{Err_{vel}}$ (%)	$\mathrm{std_{vel}}$	$\mathrm{Err_{rad}}$ (%)	$\mathrm{std_{rad}}$
Simulated data :	1.31	1.04	12.15	1.78	-	-
cine − MRI data 1 :	20.21	18.13	38.02	45.08	9.25	7.34
cine − MRI data 2 :	15.31	4.99	28.37	22.38	6.87	5.12
cine − MRI data 3 :	22.79	10.67	32.15	14.01	10.01	2.91
cine − MRI data 4 :	24.08	15.12	27.35	13.49	10.23	8.29
cine − MRI data 5 :	13.24	12.11	30.59	20.07	8.98	4.04

3 Discussion and Conclusion

The quantitative evaluation on simulated and real datasets is summarized in table (1). For validation, cine-MRI and tagging-MRI datasets are available for 5 patients. The assessment of the estimated field is performed against the motion field computed with inTag software from tagging-MRI data as gold standard. Note that except tedious post-processing techniques needed, tagging-MRI is not yet validated for clinical use. Figure 1 shows two samples of computed flow field with proposed method.

Errors computed vs. tag motion tracking (Tab. 1) are reasonable in amplitude (31.30% on average) but quite important in orientation (19.13°). This makes sense since proper motion estimation in circumferential direction would require spatial intensity gradient inside myocardium, which does not exist. This is a common problem encountered in algorithms operating on cine-MRI images, where additional constraints should be added to improve their performance, for instance incompressibility and elasticity constraints have been used in [10] to address this problem.

However, the relative error in projection on a radial reference frame computed from the middle of left ventricular cavity is much smaller (9.07% on average). Further research will be focused on improving the proposed method by adding myocardium fibre orientation constraint in data assimilation framework. This will help to recover circumferential twisting motions during cardiac contraction and the method will be extended further to 3D.

Acknowledgments. This work was supported by the 3DSTRAIN project through a grant from the French National Research Agency (ANR), Project call "Technologies for health and autonomy", grant number ANR-11-TecSan-002. The authors are grateful to Patrick Clarysse for technical help to use inTag.

References

1. Baker, S., Scharstein, D., Lewis, J.P., Roth, S., Black, M.J., Szeliski, R.: A database and evaluation methodology for optical flow. In: ICCV (2007)
2. Zhang, Z., Song, X., Sahn, D.J.: Cardiac motion estimation from 3D echocardiography with spatiotemporal regularization. In: Metaxas, D.N., Axel, L. (eds.) FIMH 2011. LNCS, vol. 6666, pp. 350–358. Springer, Heidelberg (2011)
3. Barron, J., Fleet, D., Beauchemin, S.: Performance of optical flow techniques. International Journal of Computer Vision 12, 43–77 (1994)
4. Brox, T., Bruhn, A., Papenberg, N., Weickert, J.: High accuracy optical flow estimation based on a theory for warping. In: Pajdla, T., Matas, J(G.) (eds.) ECCV 2004. LNCS, vol. 3024, pp. 25–36. Springer, Heidelberg (2004)
5. Carranza-Herrezueloa, N., Bajo, A., Sroubek, F., Santamarta, C., Cristobal, G., Santos, A., Ledesma-Carbayo, M.J.: Motion estimation of tagged cardiac magnetic resonance images using variational techniques. Computerized Medical Imaging and Graphics 34, 514–522 (2010)
6. Cohen, I.: Nonlinear variational method for optical flow computation. In: Proceedings of the 8th SCIA, pp. 523–630 (1993)
7. Deriche, R., Kornprobst, P., Aubert, G.: Optical-flow estimation while preserving its discontinuities: A variational approach. In: Asian Conference on Computer Vision, vol. 2, pp. 71–80 (1995)
8. Horn, B., Schunck, B.: Determining optical flow. Artificial Intelligence 17, 185–203 (1981)
9. Kima, Y., Martinez, A.M., Kaka, A.C.: Robust motion estimation under varying illumination. Image and Vision Computing 23, 365–375 (2005)
10. Mansi, T., Peyrat, J.-M., Sermesant, M., Delingette, H., Blanc, J., Boudjemline, Y., Ayache, N.: Physically-constrained diffeomorphic demons for the estimation of 3D myocardium strain from cine-MRI. In: Ayache, N., Delingette, H., Sermesant, M. (eds.) FIMH 2009. LNCS, vol. 5528, pp. 201–210. Springer, Heidelberg (2009)
11. Mitiche, A., Bouthemy, P.: Computation and analysis of image motion: A synopsis of current problems and methods. IJCV 19, 29–55 (1996)
12. Nagel, H.H.: Constraints for the estimation of displacement vector fields from image sequences. In: Proc. Eighth Int. Joint Conf. on Artificial Intelligence, IJCAI, pp. 945–951 (1983)
13. Papademetris, X., Sinusas, A.J., Dione, D.P., Duncan, J.S.: Estimation of 3D left ventricular deformation from echocardiography. Medical Image Analysis 5, 17–28 (2001)
14. Stiller, C., Konrad, J.: Estimating motion in image sequences. IEEE Signal Proc. Magazine 16, 70–91 (1999)
15. Tschumperlé, D., Deriche, R.: Restauration d'images vectorielles par EDP. In: 12ème Congres RFIA, vol. 17, pp. 247–256 (2000)
16. Tuyisenge, V., Albouy-Kissi, A., Cassagnes, L., Coupez, E., Merlin, C., Windyga, P., Sarry, L.: Variational myocardial tracking from cine-MRI with non-linear regularization. In: Proc. of the 10th IEEE Int. Symposium on Biomedical Imaging 2013 (ISBI 2013), San Francisco, USA. IEEE (2013)
17. Weickert, J.: On discontinuity-preserving optical flow. In: Proc. Computer Vision and Mobile Robotics Workshop, pp. 115–122 (1998)
18. Weickert, J., Bruhn, A., Brox, T., Papenberg, N.: A survey on variational optic flow methods for small displacements. Mathematics in Industry 10, 103–136 (2006)